Microglial NFκB-TNFα hyperactivation induces obsessive–compulsive behavior in mouse models of progranulin-deficient frontotemporal dementia

Grietje Krabbe[a,b,1], S. Sakura Minami[a,b,1], Jon I. Etchegaray[a,b,1], Praveen Taneja[a], Biljana Djukic[a], Dimitrios Davalos[a,2], David Le[a], Iris Lo[a], Lihong Zhan[a,b], Meredith C. Reichert[a,b], Faten Sayed[c], Mario Merlini[a], Michael E. Ward[a,b], David C. Perry[b,d], Suzee E. Lee[b,d], Ana Sias[b,d], Christopher N. Parkhurst[e], Wen-biao Gan[e], Katerina Akassoglou[a,b], Bruce L. Miller[b,d], Robert V. Farese Jr.[f,g], and Li Gan[a,b,c,3]

[a]Gladstone Institute of Neurological Diseases, University of California, San Francisco, CA 94158; [b]Department of Neurology, University of California, San Francisco, CA 94158; [c]Neuroscience Graduate Program, University of California, San Francisco, CA 94158; [d]Memory and Aging Center, Department of Neurology, University of California, San Francisco, CA 94158; [e]Skirball Institute of Biomolecular Medicine, New York University Medical Center, New York, NY 10016; [f]Department of Genetics and Complex Diseases, Harvard T. H. Chan School of Public Health, Boston, MA 02115; and [g]Department of Cell Biology, Harvard Medical School, Boston, MA 02115

Edited by Lawrence Steinman, Stanford University School of Medicine, Stanford, CA, and approved March 20, 2017 (received for review January 9, 2017)

Frontotemporal dementia (FTD) is the second most common dementia before 65 years of age. Haploinsufficiency in the progranulin (*GRN*) gene accounts for 10% of all cases of familial FTD. *GRN* mutation carriers have an increased risk of autoimmune disorders, accompanied by elevated levels of tissue necrosis factor (TNF) α. We examined behavioral alterations related to obsessive–compulsive disorder (OCD) and the role of TNFα and related signaling pathways in FTD patients with *GRN* mutations and in mice lacking progranulin (PGRN). We found that patients and mice with *GRN* mutations displayed OCD and self-grooming (an OCD-like behavior in mice), respectively. Furthermore, medium spiny neurons in the nucleus accumbens, an area implicated in development of OCD, display hyperexcitability in PGRN knockout mice. Reducing levels of TNFα in PGRN knockout mice abolished excessive self-grooming and the associated hyperexcitability of medium spiny neurons of the nucleus accumbens. In the brain, PGRN is highly expressed in microglia, which are a major source of TNFα. We therefore deleted PGRN specifically in microglia and found that it was sufficient to induce excessive grooming. Importantly, excessive grooming in these mice was prevented by inactivating nuclear factor κB (NF-κB) in microglia/myeloid cells. Our findings suggest that PGRN deficiency leads to excessive NF-κB activation in microglia and elevated TNFα signaling, which in turn lead to hyperexcitability of medium spiny neurons and OCD-like behavior.

FTD | progranulin | TNF | microglia | OCD

Frontotemporal dementia (FTD), the second most common dementia for those under 65 years of age, is characterized clinically by marked behavioral and/or language disturbance (1). Patients with FTD experience debilitating behavioral changes that commonly include social withdrawal, disinhibition, loss of sympathy/empathy, and perseverative/compulsive behaviors (2, 3). Haploinsufficiency of the progranulin (PGRN, *GRN*) gene is an important cause of familial FTD with TAR DNA-binding protein 43 (TDP-43)–positive inclusions (FTLD-TDP) (4, 5). $Grn^{-/-}$ mice develop an FTD-like pattern of behavioral disturbances: social and emotional abnormalities and only mild or late hippocampal-dependent memory dysfunction (6, 7). Pathologically, $Grn^{-/-}$ mice exhibit increased expression of proinflammatory cytokines and exacerbated microglial activation and astrogliosis, all of which are also observed in patients with FTD (8, 9). However, heterozygous *Grn* mice recapitulate some, but not most, aspects of the disease (10).

In the brain, PGRN is mainly expressed by neurons and microglia (11). Under healthy conditions, microglia survey their surroundings with their fine, branched processes to look for any change in homeostasis (12, 13). Interestingly, this surveillance involves short contacts to neuronal structures that help shape neuronal architecture (14). Upon insult, microglia transform to an activated state that is defined by morphological changes and the release of proinflammatory factors, such as chemokines and cytokines, which trigger further inflammatory and often neurotoxic responses (15). One of the major inflammatory cytokines is TNFα. Multiple lines of evidence point to PGRN as a mediator of TNFα signaling. PGRN-deficient microglia secrete large amounts of TNFα, and PGRN mutation carriers have increased levels of TNFα in plasma (9, 16). PGRN has been shown to inhibit TNFα signaling; however, whether PGRN indeed binds to these receptors directly is still debated (17, 18). TNFα has a role in inflammation and also apoptosis, cell proliferation, survival, and tissue regeneration/degeneration (19). How PGRN deficiency-induced aberrant TNFα signaling contributes to FTD-related behavioral abnormalities is unknown.

In the current study, we investigated whether excessive grooming in PGRN-deficient mice was mediated by elevated TNFα. On the network level, we show that PGRN deficiency induces hyperexcitability of medium spiny neurons (MSNs) in the nucleus accumbens, a network dysfunction associated with obsessive–compulsive disorder

Significance

Frontotemporal dementia (FTD) is a disease characterized by degeneration of the frontal and/or temporal lobes of the brain. Symptoms of FTD include changes in personality, such as loss of social awareness and impulse control. A significant portion of inherited FTD cases are due to mutations in progranulin (PGRN). These mutations lead to a decrease in the production of PGRN. How lower levels of PGRN lead to FTD is unknown. Here, we show that humans carrying PGRN mutations and mice lacking PGRN display obsessive–compulsive disorders (OCDs). In mice, OCD behavior results partially from elevated levels of the cytokine TNFα and aberrant activation of immune cells of the brain known as microglia. Our findings provide evidence that targeting innate immune pathways could be a new therapeutic strategy to treat FTD.

Author contributions: G.K., S.S.M., B.D., D.D., M.M., and L.G. designed research; G.K., S.S.M., J.I.E., P.T., D.L., I.L., L.Z., M.C.R., F.S., D.C.P., S.E.L., A.S., and B.L.M. performed research; D.D., M.E.W., C.N.P., W.-b.G., K.A., and R.V.F. contributed new reagents/analytic tools; G.K., S.S.M., J.I.E., P.T., D.C.P., S.E.L., A.S., B.L.M., and L.G. analyzed data; and G.K., S.S.M., J.I.E., and L.G. wrote the paper.

The authors declare no conflict of interest.

This article is a PNAS Direct Submission.

Freely available online through the PNAS open access option.

[1]G.K., S.S.M., and J.I.E. contributed equally to this work.

[2]Present address: Lerner Research Institute, Cleveland Clinic Foundation, Cleveland, OH 44195.

[3]To whom correspondence should be addressed. Email: lgan@gladstone.ucsf.edu.

This article contains supporting information online at www.pnas.org/lookup/suppl/doi:10.1073/pnas.1700477114/-/DCSupplemental.

(OCD)-like behaviors. Furthermore, we show that selective deletion of PGRN in microglia is sufficient to induce FTD-like behavioral abnormalities and identify an essential role of excessive NF-κB signaling in PGRN-deficient microglia.

Results

To determine whether a decrease in PGRN leads to OCD behavior in humans, we conducted a review of 35 symptomatic and presymptomatic *GRN* carriers in the University of California, San Francisco (UCSF) clinical research program. We found repetitive and compulsive behaviors in 57% of carriers (70% of 23 symptomatic and 33% of 12 presymptomatic carriers) but in none of 25 age-, sex-, and education-matched healthy controls ($P < 0.001$, Fisher's exact test) (Fig. 1*A* and Table S1). The most common repetitive or compulsive behaviors were simple stereotypes in eight subjects, repetitive checking in six subjects, repetitive grooming or personal cleanliness in three subjects, and collecting in three subjects (Fig. 1*A*). We also did voxel-based morphometry analyses of structural MRI scans of a subset of symptomatic *GRN* carriers. Twenty *GRN* mutation carriers and 42 controls matched for age, sex, and handedness were analyzed (Table S1). Consistent with previous reports (20, 21), symptomatic *GRN* mutation carriers exhibited extensive frontotemporal atrophy extending into the parietal regions; the subcortical, striatum, and amygdala showed bilateral atrophy (Fig. 1*B*).

To assess the repetitive and compulsive behavior in mice, we quantified self-grooming, a common phenotype in mouse models of OCD (22). Self-grooming time was significantly increased in $Grn^{-/-}$ mice (Fig. 2*A*). PGRN is a mediator of TNFα signaling, and increases in TNFα have been implicated in OCD (23). To directly test whether elevated TNFα levels underlie the behavioral deficits in $Grn^{-/-}$ mice, we crossed $Tnf\alpha^{-/-}$ mice with $Grn^{-/-}$ mice. Genetic removal of one allele of *Tnfα* in $Grn^{-/-}$ mice abolished the excessive grooming phenotype (Fig. 2*A*). A hot-plate test showed no difference among the groups (Fig. S1), excluding the possibility that PGRN or TNFα deficiency affected self-grooming by altering nociception. We also tested whether $Grn^{-/-}$ mice have social deficits, a hallmark of patients with autism and FTD. Using a three-chamber social interaction test, we found that, whereas control mice spent more time with another mouse than an inanimate object, $Grn^{-/-}$ mice showed no preference (Fig. S2), which suggests that $Grn^{-/-}$ mice exhibit impairments in social interaction, consistent with previous studies (6). However, reducing or deleting TNFα did not affect social interaction deficits induced by PGRN deficiency (Fig. S2). Our findings point to a specific modulatory role of TNFα in OCD-related behaviors but not autistic-like behaviors.

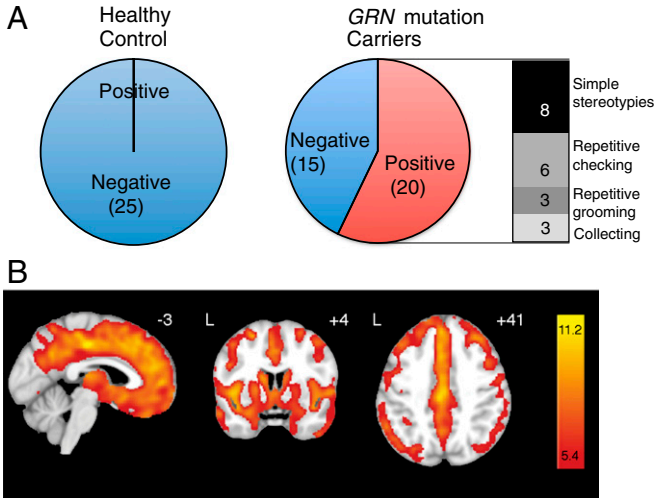

Fig. 1. *GRN* mutation carriers exhibit obsessive–compulsive behaviors and subregion gray matter atrophy. (*A*) *GRN* mutation increases repetitive and compulsive behaviors in an FTD cohort. $n = 35$ (GRN carriers), 25 (noncarriers). $P = 0.0001$, Fisher's exact test. (*B*) Gray matter atrophy in 20 of the 23 symptomatic GRN mutation carriers described in *A*. Group difference maps derived by voxel-based morphometry show extensive, bilateral atrophy of gray matter in frontotemporoparietal cortex and subcortical regions. Maps are thresholded at a t-threshold of $P < 0.05$ (corrected for familywise error). Color bars represent t-scores, and statistical maps are superimposed on the Montreal Neurological Institute template brain. The left side of the axial and coronal images corresponds to the left side of the brain.

Cortico-basal ganglia circuits, particularly the ventral striatum (nucleus accumbens), are strongly implicated in repetitive, compulsive, and impulsive behaviors. In OCD patients, deep-brain stimulation of the nucleus accumbens normalized activity in this region and restored frontostriatal network activity (24). In mice, excessive activity of striatal MSNs and reduced inhibitory inputs contribute to excessive grooming behavior (25, 26). To assess changes in the excitability of MSN neurons that could account for excessive activity, we performed whole-cell patch-clamp recordings in the core of nucleus accumbens (Fig. 2*B*). Action potential firing frequencies of MSNs were analyzed at different current intensities in WT ($Grn^{+/+}$), $Grn^{-/-}$, $Grn^{-/-}Tnf\alpha^{+/-}$, and $Grn^{-/-}Tnf\alpha^{-/-}$ mice, and action potential frequency vs. current (FI) curves were generated (Fig. 2 *C* and *D*). $Grn^{-/-}$ neurons had a higher instantaneous firing frequency than WT neurons at various current intensities, suggesting increased excitability (Fig. 2*D*). Removing one or two alleles of *TNFα* from $Grn^{-/-}$ neurons reduced the instantaneous firing frequency at 250 pA to that of WT neurons (Fig. 2*E*). TNFα deletion also reduced the elevated slope of the FI curve in $Grn^{-/-}$ neurons to the WT level (Fig. 2*F*).

$Grn^{-/-}$ mice exhibit exacerbated microglial activation and elevated levels of inflammatory cytokines, including TNFα (8, 9). Functionally, microglial processes constantly survey the environment and act as first responders to injury (12, 13). To assess how PGRN deficiency affects normal function of microglia, we compared microglial motility in $Grn^{-/-}/CX3CR1^{GFP/+}$ or $Grn^{+/+}/CX3CR1^{GFP/+}$ mice, in which microglia are labeled with green fluorescent protein (GFP), whose expression is driven by the *Cx3Cr1* promoter (27). Cortical microglia in intact brains were imaged by two-photon microscopy through a thinned-skull window (Movies S1 and S2). Baseline activity was measured by counting extensions and retractions of microglial processes in 10-min recordings (Fig. 3*A*, *Left*). The total number of extensions and retractions was significantly lower in $Grn^{-/-}$ mice than in $Grn^{+/+}$ controls (Fig. 3*A*, *Right*). Microglial processes in $Grn^{-/-}$ mice also exhibited an attenuated response to a laser-induced injury (Fig. 3 *B* and *C* and Movies S3 and S4). In a transwell assay, significantly fewer $Grn^{-/-}$ than $Grn^{+/+}$ microglia-derived cells migrated toward an ATP or ADP gradient (Fig. 3*D*). Thus, PGRN deficiency impairs normal microglia function.

Alterations in microglia/myeloid cells have been implicated in pathological grooming, but the underlying mechanism is unclear (28, 29). To determine whether microglial abnormality induced by PGRN deficiency induces excessive grooming, we crossed $Cx3Cr1\text{-}Cre^{ERT2}$ mice with $Grn^{F/F}$ mice and treated adult offspring with tamoxifen to selectively delete PGRN in microglia (30, 31). CX3CR1-cre resulted in efficient microglia-specific expression, as shown by crossing with an RFP reporter line (Fig. 4*A*). Three months after the tamoxifen treatment, PGRN expression was depleted in CD11b-positive adult microglia but not in CD11b-positive myeloid cells in the spleen (Fig. 4 *B* and *C*), confirming that PGRN deletion is restricted in adult microglia, as expected (21). We also confirmed that PGRN reduction was detected only in brain, not in blood cells or plasma (Fig. 4 *D*, *E*, and *F*). Selective deletion of PGRN in adult microglia markedly increased self-grooming, as in $Grn^{-/-}$ mice (Fig. 4*G*). These results demonstrate that PGRN-deficient microglia have a critical role in inducing OCD-like behaviors.

To further dissect how PGRN deficiency in microglia induces OCD-like behaviors, we examined the role of NF-κB signaling, a master regulator of inflammatory mediators, such as TNFα. NF-κB activation in microglia-derived cultures was quantified by expression of the reporter gene under 5xκB enhancer elements. TNFα stimulation induced a significantly stronger NF-κB activation in $Grn^{-/-}$ than $Grn^{+/+}$ cells, suggesting that PGRN deficiency increases

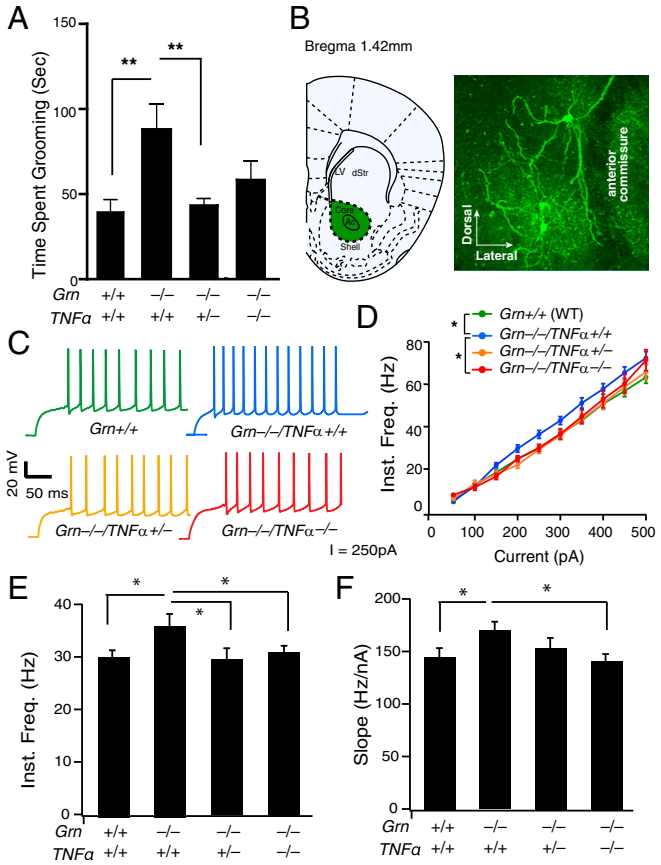

Fig. 2. Obsessive–compulsive behavior and hyperexcitability of MSNs is rescued by reducing TNFα levels in $Grn^{-/-}$ mice. (*A*) Increased self-grooming of $Grn^{-/-}$ mice is reduced to WT levels in $Grn^{-/-}Tnf\alpha^{+/-}$ mice. $n = 13, 12, 15, 10$ for $Grn^{+/+}$, $Grn^{-/-}$, $Grn^{-/-}Tnf\alpha^{+/-}$, and $Grn^{-/-}Tnf\alpha^{-/-}$ mice, respectively. $P = 0.003$, $F(3,46) = 5.276$, one-way ANOVA. $^{**}P < 0.01$; Tukey–Kramer post hoc test. (*B*) Morphology of targeted neurons in the nucleus accumbens core (*Left*) by labeling biocytin-filled cells with fluorescently conjugated streptavidin (*Right*). Representative image of more than three independent experiments. Ac, accumbens; LV, lateral ventricle; sStr, dorsal striatum. (*C*) Representative action potential firing of MSNs in $Grn^{+/+}$, $Grn^{-/-}$, $Grn^{-/-}Tnf\alpha^{+/-}$, and $Grn^{-/-}Tnf\alpha^{-/-}$ mice at 250 pA. (*D*) $Grn^{-/-}$ neurons had higher instantaneous firing frequencies than $Grn^{+/+}$, $Grn^{-/-}Tnf\alpha^{+/-}$, or $Grn^{-/-}Tnf\alpha^{-/-}$ neurons at various current intensities. (*E*) Quantification of instantaneous action potential firing frequency at 250 pA. $P = 0.0063$, one-way ANOVA. $^{*}P < 0.05$, post hoc analyses with Holm correction for multiple comparisons. (*F*) Quantification of the slopes of the FI curves shown in *D*. $^{*}P < 0.05$, one-way ANOVA and Holm correction for multiple comparisons. Number of $Grn^{+/+}$, $Grn^{-/-}$, $Grn^{-/-}Tnf\alpha^{+/-}$, *and* $Grn^{-/-}Tnf\alpha^{-/-}$ neurons (mice): 107 (16), 99 (14), 69 (9), 39 (6).

TNFα-induced NF-κB signaling (Fig. S3). We then selectively inactivated NF-κB in PGRN-deficient microglia/myeloid cells in mice. To do so, we crossed mice with lysozyme promoter-driven cre expression (*LysM-Cre*) (32) with $Grn^{F/F}$ mice and mice with a floxed *Ikbkb* gene ($Ikbkb^{F/F}$) (33), which encodes the inhibitor of the NF-κB kinase subunit β (Ikkβ) (Fig. S4). In adult microglia, lysozyme-cre expression in $Grn^{F/F}$ mice reduced PGRN expression by ∼60% and increased self-grooming significantly (Fig. 5 *A* and *B*). Selective inactivation of NF-κB in microglia/myeloid cells by deleting *Ikbkb* did not affect PGRN expression but restored grooming behavior to normal (Fig. 5 *A* and *B*). Reducing PGRN in microglia/myeloid cells also altered nesting behaviors and markedly increased marble burying, both OCD-like behaviors, and both were normalized by attenuation of NF-κB signaling in these cells (Fig. 5 *C* and *D*). The social interaction deficits induced by PGRN deficiency in myeloid cells were also prevented by inactivation of NF-κB signaling (Fig. 5*E*), supporting a central role of the innate immune pathway in PGRN-deficient FTD.

Discussion

FTD patients exhibit behavioral abnormalities, including OCD-like behaviors (34). Cortico-basal ganglia circuits, particularly ventral striatum (nucleus accumbens), are strongly implicated in the expression of repetitive, compulsive, and impulsive behaviors. Indeed, excessive activity of striatal MSNs and reduced inhibitory inputs contribute to excessive grooming behavior (25, 26). In mice lacking the synaptic scaffolding gene, *Sapap3*, that have repetitive, compulsive behavior, the baseline firing rates of MSNs in the striatum were significantly elevated, most likely due to a defect in intrastriatal inhibition (26). Using whole-cell recordings in the nucleus accumbens core, we observed hyperexcitability of PGRN-deficient MSNs, which was rescued by reduction or ablation of TNFα levels. TNFα ablation also rescued the excessive grooming, but not social deficits, in PGRN-deficient mice, linking high levels of TNFα specifically to the excessive grooming. Our findings are consistent with a recent study that showed PGRN-deficient mice exhibit excessive grooming (35). Further studies are needed to determine how TNFα and related cytokines alter the circuits to induce OCD-like behavior.

Using confocal and intravital microscopy, we found that microglia lacking PGRN are dysfunctional, with reduced baseline motility and attenuated response to injury and ATP/ADP. Moreover, selective deletion of PGRN in adult microglia, by crossing CX3CR1-CreER mice with $Grn^{F/F}$ mice, induces excessive grooming and social deficits. These findings provide strong evidence that PGRN-deficient microglia in adult brain play a critical role in FTD-related phenotypes. Distinct from previous findings that linked excessive grooming with the Hoxb8 mutation (36) and bone marrow cells, our findings link excessive grooming to dysfunctional adult microglia. We further identified an instrumental role of NF-κB hyperactivation signaling in PGRN-deficient microglia. Selective inhibition of NF-κB in myeloid cells prevented not only excessive grooming, but also other FTD-like phenotypes, including social interaction deficits. Unlike TNFα, which seems to mediate excessive grooming, but not social deficits, NF-κB is a master regulator of inflammatory responses, and its hyperactivation would alter many pathways in PGRN-deficient mice. As a result, inhibition of NF-κB in myeloid cells abolished all FTD-related behaviors we tested. The downstream pathways responsible for various behavioral alterations in PGRN-deficient mice remain to be determined.

Our findings that PGRN substantially affects microglial function and that disruption of *Grn* expression in microglia is sufficient to induce OCD-like behavior provide insight into how PGRN deficiency induces FTD. Inhibition of the NF-κB pathway, in particular TNFα, is a potential therapeutic approach for reducing MSN hyperexcitability and associated OCD-like behaviors in PGRN-deficient FTD.

Methods

Patient Behavior and Voxel-Based Morphometry Analyses.

Participants. Written informed consent was obtained from patients or surrogates according to procedures approved by the UCSF Committee on Human Research. All *GRN* mutation carriers and healthy controls were clinically assessed by a behavioral neurologist and a neuropsychologist within 180 d of MRI scanning. Clinical diagnoses were made at a multidisciplinary consensus conference (Table S1). Genetic analysis for the *GRN* mutation was as described (4). Repetitive and compulsive behaviors were routinely noted in clinician research summaries and measured with the aberrant motor behavior scale of the Neuropsychiatric Inventory (37). Simple stereotypes are characterized by picking clothing or skin, tapping fingers or feet, rubbing hands or legs, and nail biting. Aberrant motor behaviors seen in these patients also include repetitive checking, repetitive grooming or personal cleanliness (brushing teeth, hand washing, shaving), and collecting. Other repetitive activities were less common in this group of patients (e.g., list making, compulsive visual art, verbal stereotypies, pacing, superstitious fears and rituals, cleaning, ordering or arranging, repetitive purchases, or preoccupation with narrow habits or interests).

Voxel-based morphometry analyses. A review of the University of California, San Francisco Memory and Aging Center database identified 20 symptomatic *GRN* carriers who had a structural MRI scan. The clinical diagnosis was FTD in 12 of the carriers, cortico-basal syndrome in 2, primary progressive aphasia in 3, and Alzheimer's disease in 3. Thirteen GRN carriers and 30 controls

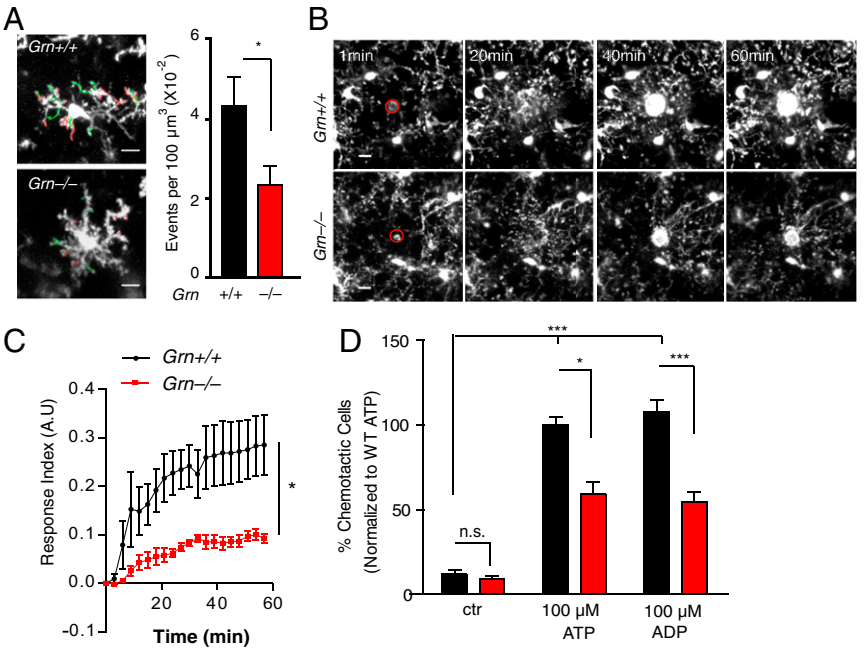

Fig. 3. PGRN-deficient microglia are functionally impaired. (*A*) Baseline motility of $Grn^{+/+}$/*Cx3Cr1+/GFP* and $Grn^{-/-}$/*Cx3Cr1+/GFP* microglia was measured by intravital two-photon microscopy; the number of process extensions (Green) and retractions (red) were quantified over 10 min. $n = 6$, six regions of interest (ROIs) from 4, 5 mice. $^{*}P < 0.05$, unpaired *t* test. (Scale bar: 10 μm.) (*B*) Representative projections at different times show the response to a laser ablation (red circle) in $Grn^{+/+}$*Cx3Cr1+/GFP* (*Top*) or $Grn^{-/-}$*Cx3Cr1+/GFP* mice (*Bottom*). (Scale bar: 10 μm.) (*C*) The response of microglia to a laser ablation was measured over 60 min. $n = 6$, 7 ROIs from five mice per genotype. Two-way-ANOVA, $P < 0.0001$, genotype effects. $^{*}P < 0.05$, Bonferroni post hoc test. (*D*) The chemotactic response of primary microglia from $Grn^{+/+}$ or $Grn^{-/-}$ mice toward 100 μm ATP or ADP was measured by a transwell assay. $n = 17$, 35 ROIs from four independent experiments. $^{*}P < 0.05$; $^{***}P < 0.001$; n.s., not significant. Kruskal–Wallis test and Dunn's multiple comparison post hoc test.

underwent MRI scanning with a Siemens Tim Trio 3T scanner; T1-weighted images were obtained with volumetric magnetization-prepared rapid gradient echo sequences (repetition time, 2,300 ms; echo time, 2.98 ms; flip angle, 9°; 160 sagittal slices; matrix size, 240 × 256; voxel size, 1 mm^3). Seven GRN carriers and 12 controls underwent MRI scanning with a 1.5T Magnetom Vision system (Siemens); T1-weighted images of the entire brain were obtained with volumetric magnetization-prepared rapid gradient echo sequences (repetition time, 10 ms; echo time, 4 ms; inversion time, 300 ms; flip angle, 15°; coronal orientation perpendicular to the double spin echo sequence, 1 × 1-mm^2 in-plane resolution, and 1.5-mm slab thickness). Voxel-based morphometry was done with SPM12 (www.fil.ion.ucl.ac.uk/spm/). T1-weighted images were preprocessed by standard spatial normalization in the SPM12 segment module, using the six standard tissue probability maps with a light cleanup. Standard affine regularization with the ICBM European brain template and warping regularization with the default parameters were used. Images of gray matter and white matter were segregated. Gray matter images were smoothed with an 8-mm full-width at half-maximum isotropic Gaussian kernel. Smoothed gray matter maps of *GRN* mutation carriers and controls were compared with two-sample *t* tests. Nuisance covariates included age, sex, handedness, total intracranial volume, and scanner. Voxel-based morphometry analyses were thresholded at $P < 0.05$ (corrected for familywise error).

Mice. *TNFα, LysM-cre, CX3CR1-cre-ETR, Ikbkb$^{F/F}$, Cx3cr1$^{GFP/+}$*, and $Grn^{-/-}$ mice were on a C57B6 background. $Grn^{F/F}$ mice (9) were on a C57B/6J mixed background. To remove *Grn* alleles from myeloid cells, $Grn^{F/F}$ mice (9) were crossed with mice in which CreER recombinase expression was driven by the fractalkine receptor (Cx3Cr1) promoter (30). In 2- to 3-mo-old *Cx3Cr1-CreER^{+}/Grn$^{F/F}$* mice, Cre expression was induced by i.p. injection of tamoxifen (2 mg/d in corn oil) for 5 or 10 d. To confirm microglia-specific Cre expression, *Cx3Cr1-CreER^{+}* mice were crossed with *RFP$^{F/F}$* mice and treated with tamoxifen. For rescue experiments, $Grn^{F/F}$ mice or $Grn^{-/-}$ mice were crossed either with mice expressing floxed *Ikbkb* and Cre recombinase under the LysM promoter to abolish NF-κB signaling specifically in myeloid cells (32, 38) or with TNFα knockout mice (The Jackson Laboratory) to deplete proinflammatory TNFα signaling. For identification of microglia in in vivo imaging experiments, *Cx3cr1$^{GFP/+}$* mice (27) were crossed with $Grn^{-/-}$ mice to obtain PGRN-deficient and WT mice that expressed GFP heterozygously in myeloid cells. No more than five same-sex mice were housed in a single cage. All animal procedures were consistent with guidelines approved by the Institutional Animal Care and Use Committee of the University of California, San Francisco.

Behavior Tests. All mice were housed in a pathogen-free barrier facility with a 12 h light/12 h dark cycle and ad libitum access to food and water. Behavioral experiments were done during daylight hours. Investigators who performed the behavior tests and subsequent manual scoring were blinded to the genotypes of the mice. No randomization was used. Mice for experiments were chosen in semirandom, interleaving manner. All mice tested behaviorally had not been subject to prior drug administration or surgery. Some cohorts participated in multiple noninvasive behavioral tests.

Grooming. The protocol for analyzing self-grooming behavior was adapted from Yang et al. (22). Mice were tested between 1200 hours and 1600 hours after 10 min of habituation to an empty housing cage covered with a lid. Then mice were videotaped for 10 min.

Nesting. Mice were placed in a new housing cage containing two cotton nestlets for 7 h. Nest quality was scored under blinded conditions as described (39). A score of 0 indicated a nestlet untouched after 7 h. A score of 5 indicated a nest with complete dome and only one small entry hole. Unfinished nests were scored 1, 2, or 3, depending on the height of the walls.

Social interaction. Mice were allowed to freely explore an empty three-chambered box containing two empty wire cups in the outer chambers. After 10 min, a stranger mouse was placed in one of the cups and an inanimate object in the other, and time spent sniffing each cup was quantified for 10 min. Data are presented as the ratio of time spent sniffing the mouse cup to time spent sniffing the object cup.

Marble burying. Twelve glass marbles were distributed in a 4 × 3 grid in a new housing cage with double bedding material. Each mouse was allowed to explore the cage for 30 min in dim light. A marble was considered buried if it was less than 50% was visible.

Hot plate test. Mice were placed in a glass cylinder on a 52 °C hot plate. Latency to a nociceptive response (hind paw lick, flick, or jump) was measured, and mice were immediately removed from the apparatus. If a nociceptive response was not seen within 30 s, the test was stopped.

Electrophysiological Recordings. The recordings and subsequent analyses were performed by an investigator blinded to the genotypes of the mice. The mean ages of $Grn^{+/+}$, $Grn^{-/-}$, $Grn^{-/-}Tnf\alpha^{+/-}$, and $Grn^{-/-}Tnf\alpha^{-/-}$ mice were 351, 332, 369, and 358 d, respectively. Mice were anesthetized with isoflurane and cardiac-perfused with ice-cold *N*-methyl-D-glucamine (NMDG)-based artificial cerebrospinal fluid (ACSF) (93 mM *N*-methyl-D-glucamine, 2.5 mM KCl, 1.25 mM NaH_2PO_4, 30 mM $NaHCO_3$, 20 mM Hepes, 25 mM glucose, 2 mM thiourea, 5 mM Na-ascorbate, 3 mM Na-pyruvate, 12 mM *N*-acetyl-L-cysteine, 0.5 mM $CaCl_2$, and 10 mM $MgSO_4$; 295 mOsm) designed to obtain healthy slices from aged mice (40). The brain was quickly extracted, allowed to cool for 20 s in ice-cold NMDG-ACSF, and cut into 300-μm coronal sections with a vibratome (Thermo Scientific). Slices containing the nucleus accumbens (identified by using the anterior commissure and olfactory limb as landmarks) were incubated in NMDG-ACSF for 10 min at 35 °C, in Hepes-based ACSF (92 mM NaCl, 2.5 mM KCl, 1.25 mM NaH_2PO_4, 30 mM $NaHCO_3$, 20 mM Hepes, 25 mM glucose, 2 mM thiourea, 5 mM Na-ascorbate, 3 mM Na-pyruvate, 12 mM *N*-acetyl-L-cysteine, 2 mM $CaCl_2$, and 2 mM $MgSO_4$; 305 mOsm) at room temperature for 1 h, and in ACSF (126 mM NaCl, 26 mM $NaHCO_3$, 3.0 mM KCl, 1.25 mM NaH_2PO_4, 2.0 mM $CaCl_2$, 2 mM $MgCl_2$, and 20 mM dextrose; 320 mOsm) at room temperature for at least 45 min. All solutions were constantly bubbled with a mixture of 95% O_2 and

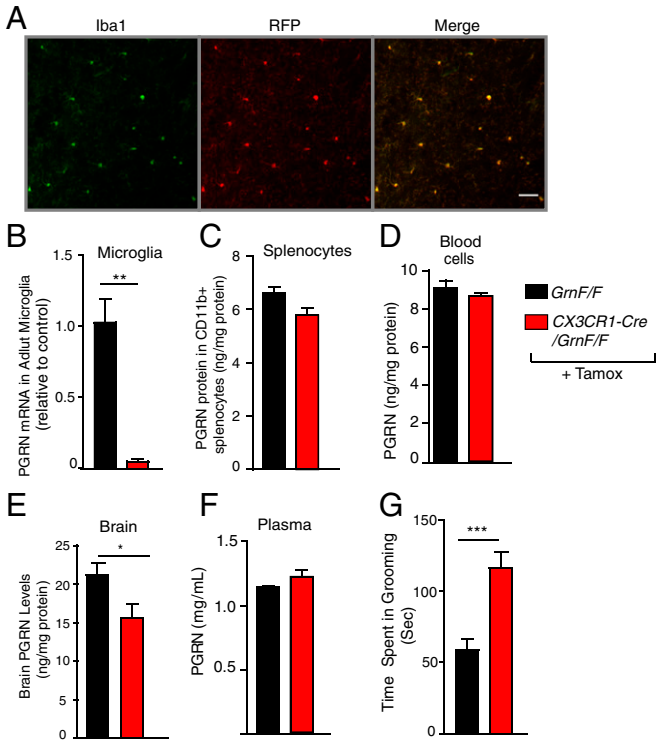

Fig. 4. Microglial PGRN deficiency induces excessive self-grooming. (*A*) Representative pictures of RFP-expressing microglia in tamoxifen (Tamox)-injected *Cx3Cr1-CreERT2/RFPF/F* mice. Image shows colocalization (*Right*, merge) of Iba1 immunoreactivity (*Left*, microglia, green) and Cre-driven RFP expression (*Center*, red). Representative of two independent experiments. (Scale bar: 40 μm.) (*B–D*) Tamoxifen injection in *GrnF/F/Cx3Cr1-CreERT2* mice induces selective deletion of PGRN in microglia (*B*), but not in spleen macrophages (*C*) or blood cells (*D*). PGRN mRNA in microglia was measured with quantitative reverse transcription (qRT-PCR). PGRN proteins were measured with ELISA. $n = 3$ mice per genotype (*B*), $n = 4$ mice/genotype (*C* and *D*). $^{**}P < 0.01$, unpaired t test. (*E* and *F*) Tamoxifen injection reduces PGRN in the brain, but not in plasma of *GrnF/FCx3Cr1-CreERT2* mice. PGRN levels were measured by ELISA. $n = 12$ mice per genotype (*E*), $n = 4$ mice per genotype (*F*). $^{*}P < 0.05$, unpaired t test. (*G*) Tamoxifen-injected *GrnF/F/Cx3Cr1-CreERT2* mice show increased self-grooming time at 8 to 10 mo of age. $n = 17, 9$. $^{***}P < 0.001$, unpaired t test.

5% CO_2, pH 7.3 to 7.35. Slices were transferred to a submerged recording chamber and continuously perfused with ACSF at 33 °C during recording. Patch pipettes with a tip resistance of 6–8 MΩ were filled with a solution consisting of 20 mM KCl, 100 mM K-gluconate, 10 mM Hepes, 4 mM Mg-ATP, 0.3 mM Na-GTP, 10 mM Na-phosphocreatine, and 0.2% biocytin (300 mOsm).

Neurons were identified visually, and whole-cell recordings were obtained with glass pipette electrodes filled with internal solution. The membrane potential was held at –75 mV (resting membrane potential was about –80 mV), and 1.5-s current pulses of different amplitudes were elicited in a pseudorandom sequence to generate an FI curve (action potential frequency vs. current). The slopes of FI curves were measured by fitting a straight line between the current threshold and 200 pA above the current threshold for each curve and averaging across neurons. For statistical analysis and analyses of spike counts and shape parameters, we used custom-written software in Igor Pro (WaveMetrics) and Python. The custom code is available under the section "code availability." Neurons with series resistance >30 MΩ or membrane resistance >386 MΩ (75th percentile + 1.5 × interquartile range) were excluded from analysis.

In Vivo Imaging. For live imaging with a two-photon microscope, thinned-skull windows were made in *Cx3cr1*$^{GFP/+}$*Grn*$^{+/+}$ and *Cx3cr1*$^{GFP/+}$*Grn*$^{-/-}$ mice as described (13). Detailed methods are described in the *SI Methods*.

Quantifying Microglial Chemotaxis. To study the chemotaxis of primary microglial cells, we used 24-well cell-culture inserts (pore size 8 μm; Falcon). ADP or ATP was diluted in serum-free DMEM (DMEM, final concentration, 100 μM) and applied to a 24-well cell-culture plate (Corning). Freshly harvested primary microglia (10^5) were placed on a cell-culture insert on wells containing serum-free DMEM (control), ATP, or ADP. After incubation at 37 °C for 5 h, the inserts were washed, and the cells were fixed and stained with Diff-Quik (Medion Diagnostics). Nonmigrated cells on the upper surface of each insert were removed with a cotton swab. The rate of migration was determined by counting cells in four microscopic fields per well with a Leica DM5000B microscope equipped with a Leica DFC310 FX camera. All experiments were done in duplicate, and numbers were normalized to a control group (WT microglia in serum-free DMEM).

Blood and Spleen Cell Harvest. Mice were deeply anesthetized with Avertin. Detailed methods are described in the *SI Methods*.

Isolation of Microglia from Adult Mouse Brain. Adult microglia were isolated from tamoxifen-injected *Cx3Cr1Cre*^{ERT2}*Grn*$^{F/F}$ or *Grn*$^{F/F}$ mice as described (41) with minor modifications. Detailed methods are described in the *SI Methods*.

Primary Mouse Microglia. Primary cultures were prepared from *Grn*$^{+/+}$ or *Grn*$^{-/-}$ mice on postnatal day 0 or 1. Detailed methods are described in the *SI Methods*.

Quantitative Real-Time PCR. RNA was extracted from cortices or from freshly isolated adult microglia. Expression was normalized to that of GAPDH and expressed as fold change relative to the average value in WT mice. Detailed methods are described in the *SI Methods*.

Protein Extraction and ELISAs. Protein extraction and mouse PGRN levels were detected by ELISA as described (42). Detailed methods are described in the *SI Methods*.

Immunohistochemistry. For identification of microglia, mouse brain sections were permeabilized in Tris-buffered saline with 0.5% Triton X-100, blocked with

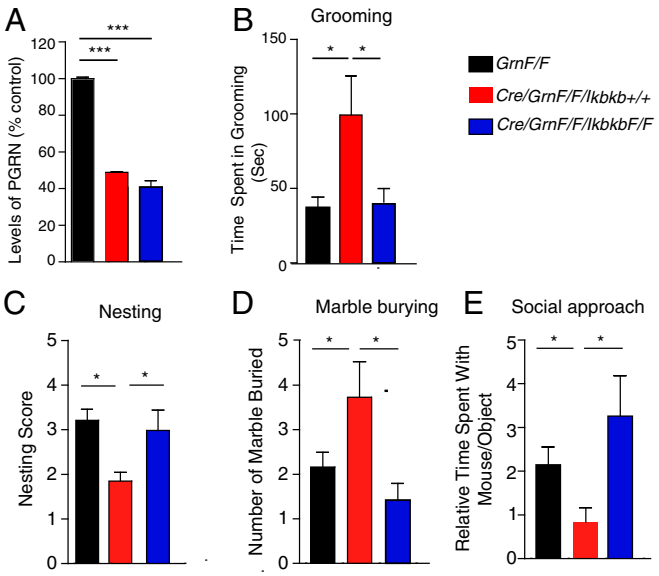

Fig. 5. Inhibition of NF-κB signaling abolished FTD-like behavioral abnormalities induced by microglial PGRN deficiency. (*A*) PGRN mRNA levels in CD11b^{+} microglia from *GrnF/F* or *LysM-Cre/GrnF/F* with or without *Ikbkb*, determined by qRT-PCR. $n = 4$ mice per group. $^{***}P < 0.001$, one-way ANOVA and Tukey's post hoc test. (*B*) Attenuation of NF-κB signaling in PGRN-deficient microglia/myeloid cells in *LysM-Cre/GrnF/FIkbkbF/F* mice restored the excessive self-grooming in *LysM-Cre/GrnF/F* mice to *GrnF/F* (WT) levels. $n = 7$ to 9 mice per genotype. $^{*}P < 0.05$, one-way ANOVA and Bonferroni post hoc test. (*C*) Attenuation of NF-κB signaling in microglia/myeloid cells restored the nesting to WT (*GrnF/F*) levels. $n = 26, 10, 12$. $^{*}P < 0.05$, one–way ANOVA with Newman–Keuls post hoc test. (*D*) Attenuation of NF-κB signaling in microglia/myeloid cells restored the marble burying to WT (*GrnF/F*) levels. $n = 31, 11, 12$. $^{*}P < 0.05$, one-way ANOVA, one-way ANOVA with Newman–Keuls post hoc test. (*E*) Attenuation of NFκB signaling in microglia/myeloid cells restored social interaction to WT (GrnF/F) levels. $n = 31, 11, 12$. $^{*}P < 0.05$, one-way ANOVA, one-way ANOVA with Newman–Keuls post hoc test.

10% normal goat or donkey serum (Jackson Immunoresearch), and stained with rabbit anti-Iba1 (1:750; Wako). Immunoreactive structures were detected with Alexa-488 Fluor goat or donkey anti-rabbit antibody (Invitrogen). Slices were washed and stained for 30 min with Hoechst 33258 (1:10000; Sigma) and mounted for analysis by confocal microscopy. Images were acquired with a Nikon ECLIPSE Ti 2000 spinning-disk confocal microscope.

NF-κB Reporter Assay. *Grn* WT or *Grn*$^{-/-}$ primary microglia cells were transduced with 5xκB-GFP or pGreenFire-5xκB lentivirus expressing both GFP and luciferase as reporters to assess NF-κB activity. Cells were treated with recombinant TNFα (100 mg/mL; R&D Systems) for 8 h and imaged, or they were lysed in luciferase assay buffer (Promega) and analyzed for luciferase activity with a Victor luminometer (Perkin-Elmer).

Statistical Analysis. Prism v.5 (GraphPad), STATA (StataCorp LP), or IgorPro (Wavemetrics) was used for data analysis. All values in the figures are expressed as means ± SEM. Sample sizes were determined based on our previous experience or published literature. For human studies, the sample size depended on the availability of the patients at the time of the study. Outliers were excluded according to criteria defined a priori (e.g., >2 SD above or below). Differences between means were assessed by unpaired, two-tailed *t* test (parametric data) or Mann–Whitney *U* test (nonparametric data). Differences among multiple means were assessed by one-way ANOVA, followed by all pairwise comparisons among genotypes (with Tukey–Kramer or Bonferroni correction for multiple comparisons) as indicated. The Kruskal–Wallis test was used to compare nonparametric data. An F test was used to compare variances on every dataset. If variances were significantly different, Welch's correction was applied. The analyses of the intrinsic excitability data were carried out using custom scripts in IgorPro. *P* values were corrected for multiple comparisons using the method of Holm.

Code Availability. The code for analyzing the F/I slope is available at https://github.com/praveen-taneja/data-analysis-igor-pro-wavemetrics.

ACKNOWLEDGMENTS. We thank Yungui Zhou, Vivian Shen, and Robert Chen for technical help; Drs. Eric Roberson, Brian Warmus, Anatol Kreitzer, Laura Mitic, and Seo-hyun Cho for technical advice and insightful discussion; and Dr. Michael Karin (University of California, San Diego) for *IkbkbF/F* mice. Genotyping information of human samples was provided by Drs. Giovanni Coppola and Dan Geschwind (University of California, Los Angeles). This work was supported in part by the Consortium for Frontotemporal Dementia (L.G., R.V.F., and S.E.L.), NIH Grants 1R01AG036884 and R01AG051390 (to L.G.), K23 AG039414 (to S.E.L.), and F32NS076239 (to S.S.M.), a postdoctoral fellowship from the German Academic Exchange Service (to G.K.), NIH Grants R35 NS097976 (to K.A.), 1R01NS087198 (to W.-b.G.), and NIH/NCRR Grant CO6 RRO18928 (a facility grant to The J. David Gladstone Institutes). Behavioral data were obtained with the help of the Gladstone Neurobehavioral Core (supported by NIH Grant P30NS065780). Human studies were supported by ADRC Grant P50 AG023501 (to B.L.M.) and PPG Grant P01 AG019724 (to B.L.M.).

1. Vossel KA, Miller BL (2008) New approaches to the treatment of frontotemporal lobar degeneration. *Curr Opin Neurol* 21:708–716.
2. Viskontas IV, Possin KL, Miller BL (2007) Symptoms of frontotemporal dementia provide insights into orbitofrontal cortex function and social behavior. *Ann N Y Acad Sci* 1121:528–545.
3. Rascovsky K, et al. (2011) Sensitivity of revised diagnostic criteria for the behavioural variant of frontotemporal dementia. *Brain* 134:2456–2477.
4. Baker M, et al. (2006) Mutations in progranulin cause tau-negative frontotemporal dementia linked to chromosome 17. *Nature* 442:916–919.
5. Cruts M, et al. (2006) Null mutations in progranulin cause ubiquitin-positive frontotemporal dementia linked to chromosome 17q21. *Nature* 442:920–924.
6. Yin F, et al. (2010) Behavioral deficits and progressive neuropathology in progranulin-deficient mice: A mouse model of frontotemporal dementia. *FASEB J* 24:4639–4647.
7. Ghoshal N, Dearborn JT, Wozniak DF, Cairns NJ (2012) Core features of frontotemporal dementia recapitulated in progranulin knockout mice. *Neurobiol Dis* 45: 395–408.
8. Yin F, et al. (2010) Exaggerated inflammation, impaired host defense, and neuropathology in progranulin-deficient mice. *J Exp Med* 207:117–128.
9. Martens LH, et al. (2012) Progranulin deficiency promotes neuroinflammation and neuron loss following toxin-induced injury. *J Clin Invest* 122:3955–3959.
10. Filiano AJ, et al. (2013) Dissociation of frontotemporal dementia-related deficits and neuroinflammation in progranulin haploinsufficient mice. *J Neurosci* 33:5352–5361.
11. Daniel R, Daniels E, He Z, Bateman A (2003) Progranulin (acrogranin/PC cell-derived growth factor/granulin-epithelin precursor) is expressed in the placenta, epidermis, microvasculature, and brain during murine development. *Dev Dyn* 227:593–599.
12. Nimmerjahn A, Kirchhoff F, Helmchen F (2005) Resting microglial cells are highly dynamic surveillants of brain parenchyma in vivo. *Science* 308:1314–1318.
13. Davalos D, et al. (2005) ATP mediates rapid microglial response to local brain injury in vivo. *Nat Neurosci* 8:752–758.
14. Tremblay ME, Lowery RL, Majewska AK (2010) Microglial interactions with synapses are modulated by visual experience. *PLoS Biol* 8:e1000527.
15. Hanisch UK, Kettenmann H (2007) Microglia: Active sensor and versatile effector cells in the normal and pathologic brain. *Nat Neurosci* 10:1387–1394.
16. Miller ZA, et al. (2013) TDP-43 frontotemporal lobar degeneration and autoimmune disease. *J Neurol Neurosurg Psychiatry* 84:956–962.
17. Tang W, et al. (2011) The growth factor progranulin binds to TNF receptors and is therapeutic against inflammatory arthritis in mice. *Science* 332:478–484.
18. Chen X, et al. (2013) Progranulin does not bind tumor necrosis factor (TNF) receptors and is not a direct regulator of TNF-dependent signaling or bioactivity in immune or neuronal cells. *J Neurosci* 33:9202–9213.
19. Kalliolias GD, Ivashkiv LB (2016) TNF biology, pathogenic mechanisms and emerging therapeutic strategies. *Nat Rev Rheumatol* 12:49–62.
20. Whitwell JL, et al. (2012) Neuroimaging signatures of frontotemporal dementia genetics: C9ORF72, tau, progranulin and sporadics. *Brain* 135:794–806.
21. Rohrer JD, et al. (2010) Distinct profiles of brain atrophy in frontotemporal lobar degeneration caused by progranulin and tau mutations. *Neuroimage* 53:1070-6.
22. Yang M, et al. (2012) Reduced excitatory neurotransmission and mild autism-relevant phenotypes in adolescent Shank3 null mutant mice. *J Neurosci* 32:6525–6541.
23. Konuk N, et al. (2007) Plasma levels of tumor necrosis factor-alpha and interleukin-6 in obsessive compulsive disorder. *Mediators Inflamm* 2007:65704.
24. Figee M, et al. (2013) Deep brain stimulation restores frontostriatal network activity in obsessive-compulsive disorder. *Nat Neurosci* 16:386–387.
25. Ahmari SE, et al. (2013) Repeated cortico-striatal stimulation generates persistent OCD-like behavior. *Science* 340:1234–1239.
26. Burguière E, Monteiro P, Feng G, Graybiel AM (2013) Optogenetic stimulation of lateral orbitofronto-striatal pathway suppresses compulsive behaviors. *Science* 340: 1243–1246.
27. Jung S, et al. (2000) Analysis of fractalkine receptor CX$_{(3)}$CR1 function by targeted deletion and green fluorescent protein reporter gene insertion. *Mol Cell Biol* 20: 4106–4114.
28. Zhan Y, et al. (2014) Deficient neuron-microglia signaling results in impaired functional brain connectivity and social behavior. *Nat Neurosci* 17:400–406.
29. Greer JM, Capecchi MR (2002) Hoxb8 is required for normal grooming behavior in mice. *Neuron* 33:23–34.
30. Parkhurst CN, et al. (2013) Microglia promote learning-dependent synapse formation through brain-derived neurotrophic factor. *Cell* 155:1596–1609.
31. Yona S, et al. (2013) Fate mapping reveals origins and dynamics of monocytes and tissue macrophages under homeostasis. *Immunity* 38:79–91.
32. Clausen BE, Burkhardt C, Reith W, Renkawitz R, Förster I (1999) Conditional gene targeting in macrophages and granulocytes using LysMcre mice. *Transgenic Res* 8: 265–277.
33. Greten FR, et al. (2004) IKKbeta links inflammation and tumorigenesis in a mouse model of colitis-associated cancer. *Cell* 118:285–296.
34. Perry DC, et al. (2012) Voxel-based morphometry in patients with obsessive-compulsive behaviors in behavioral variant frontotemporal dementia. *Eur J Neurol* 19:911–917.
35. Lui H, et al. (2016) Progranulin deficiency promotes circuit-specific synaptic pruning by microglia via complement activation. *Cell* 165:921–935.
36. Chen SK, et al. (2010) Hematopoietic origin of pathological grooming in Hoxb8 mutant mice. *Cell* 141:775–785.
37. Cummings JL, et al. (1994) The Neuropsychiatric Inventory: Comprehensive assessment of psychopathology in dementia. *Neurology* 44:2308–2314.
38. Cho IH, et al. (2008) Role of microglial IKKbeta in kainic acid-induced hippocampal neuronal cell death. *Brain* 131:3019–3033.
39. Deacon RM (2006) Assessing nest building in mice. *Nat Protoc* 1:1117–1119.
40. Ting JT, Daigle TL, Chen Q, Feng G (2014) Acute brain slice methods for adult and aging animals: Application of targeted patch clamp analysis and optogenetics. *Methods Mol Biol* 1183:221–242.
41. Hickman SE, Allison EK, El Khoury J (2008) Microglial dysfunction and defective beta-amyloid clearance pathways in aging Alzheimer's disease mice. *J Neurosci* 28: 8354–8360.
42. Minami SS, et al. (2014) Progranulin protects against amyloid β deposition and toxicity in Alzheimer's disease mouse models. *Nat Med* 20:1157–1164.